J Mater Sci (2010) 45:4097–4110
DOI 10.1007/s10853-010-4498-0

Yield stress of SiC reinforced aluminum alloy composites

Min Song · Yuehui He · Shanfeng Fang

Received: 10 October 2009 / Accepted: 7 April 2010 / Published online: 21 April 2010

Abstract This article develops a constitutive model for the yield stress of SiC reinforced aluminum alloy composites based on the modified shear lag model, Eshelby's equivalent inclusion approach, and Weibull statistics. The SiC particle debonding and cracking during deformation have been incorporated into the model. It has been shown that the yield stress of the composites increases as the volume fraction and aspect ratio of the SiC particles increase, while it decreases as the size of the SiC particles increases. Four types of aluminum alloys, including pure aluminum, Al–Mg–Si alloy, Al–Cu–Mg alloy, and Al–Zn–Mg alloy, have been chosen as the matrix materials to verify the model accuracy. The comparisons between the model predictions and the experimental counterparts indicate that the present model predictions agree much better with the experimental data than the traditional modified shear lag model predictions. The present model indicates that particle failure has important effect on the yield stress of the SiC reinforced aluminum alloy composites.

Introduction

The incorporation of SiC platelets or whiskers in an aluminum alloy matrix results in an increase in the elastic modulus and yield stress. In general, the strengthening effect has been primarily attributed to two factors in various earlier investigations. One is the shear lag model and the modified shear lag model [1–5] based on the Al matrix transferring the applied stress to the hard SiC reinforcement, while the other is the quench strengthening model [6–8] based on the increase in the dislocation density of the aluminum alloy matrix due to the difference in the coefficient of thermal expansion between the hard SiC reinforcement and the Al matrix. These two models, in some way, have successfully been applied to predict the elastic modulus and yield stress of the composites. However, both the shear lag model and the quench strengthening model did not include the effects of particle debonding or particle cracking on the yield stress of the composites, a phenomenon being generally observed during deformation of the SiC reinforced aluminum alloy composites. It is believed that both the particle cracking and particle debonding have important effects on the yield stress of the composites since the applied stress cannot be transferred to the failed SiC reinforcements.

Many previous studies [9–12] indicated that both the particle cracking and particle debonding can be described by Weibull statistics. However, applying the Weibull statistics to predict the particle debonding and particle cracking requires the internal stress on the SiC reinforcements be calculated. A previous study [13] indicated that the internal stress on the short fiber metal matrix composites can be determined using Eshelby's equivalent inclusion approach, which provides a way to calculate the yield stress of the composites by considering the particle cracking and particle debonding. In this article, we present a new approach to study the yield stress of the SiC reinforced aluminum alloy composites. Both the particle cracking and particle debonding have been incorporated into the model based on the Weibull statistics and the Eshelby's equivalent inclusion approach, while the macro yield stress of the composites has been calculated using the modified shear lag model.

M. Song (✉) · Y. He · S. Fang
State Key Laboratory of Powder Metallurgy, Central South University, Changsha 410083, People's Republic of China
e-mail: min.song.th05@alum.dartmouth.org

Model description

The modified shear lag model

The modified shear lag model [3, 4] was developed to predict discontinuous composite strength based on load being transferred by shear. For SiC reinforced aluminum alloy composites, the predicted yield stress (σ_{cy}) can be expressed as [3, 4]

$$\sigma_{cy} = \sigma_{my}[f_p(A+2)/2 + f_m], \quad (1)$$

where A is the aspect ratio (defined as length/diameter), f_p is the volume fraction of the SiC reinforcements, f_m is the volume fraction of the matrix, and σ_{my} is the matrix yield stress. It should be noted that the application of Eq. 1 requires the volume fraction of the reinforcements to be less than that of the matrix ($f_p < f_m$). Since the volume fraction of the reinforcements plus that of the matrix equals one ($f_p + f_m = 1$), $f_p < f_m$ indicates that f_p is <50%. It should also be noted that dislocations bypassing the reinforcements can increase the yield stress. This strengthening mechanism is the Orowan strengthening effect. Assuming that the SiC particles are equiaxed, the Orowan strengthening $\Delta\sigma_{or}$ can be expressed as [8]

$$\Delta\sigma_{or} = 2G\boldsymbol{b}/L, \quad (2)$$

where $L = 0.6d(2\pi/f_p)^{1/2}$ is the inter-particle spacing (assuming that particles are uniformly distributed), d is the granularity of the SiC particles (note that the granularity is defined as the square root of the result of length times diameter), $\boldsymbol{b}$ is the Burgers vector, and G is the matrix shear modulus. Thus, by considering the Orowan strengthening effect, the yield stress of the composites can be expressed as

$$\sigma_{cy} = \sigma_{my}[f_p(A+2)/2 + f_m] + \Delta\sigma_{or} \quad (3)$$

The matrix yield stress, σ_{my}, can be calculated by combining the effect of the matrix intrinsic yield stress (σ_{in}), the quenching strengthening (σ_{qs}), the grain refinement strengthening (σ_{grs}), and the geometrically necessary dislocation strengthening (σ_{gnds}). Thus, the yield stress of the composites can be expressed as

$$\sigma_{cy} = (\sigma_{in} + \sigma_{qs} + \sigma_{grs} + \sigma_{gnds})[f_p(A+2)/2 + f_m] + \Delta\sigma_{or} \quad (4)$$

The quench strengthening results from the generation of the dislocations due to the large difference in thermal expansion between the matrix and the reinforcements. The generation of the dislocations is generally caused by quenching from recrystallization or solution treatment temperature. The increment of the yield stress can be expressed as [7]

$$\sigma_{qs} = \alpha_1 G\boldsymbol{b}\rho^{1/2} \quad (5)$$

$$\rho = \frac{4f_p\Delta T\Delta C}{b(1-f_p)}\left(\frac{1}{t_1}+\frac{1}{t_2}+\frac{1}{t_3}\right), \quad (6)$$

where ΔT is the temperature change; ΔC is the thermal mismatch; t_1, t_2, and t_3 are the three-dimensional coefficients of the particles (the maximum size of the particles along three perpendicular directions); ρ is the dislocation density; and α_1 is the dislocation strengthening coefficient. A previous study [14] indicated that for pure metals, $\alpha_1 = 0.5$–0.8; for solution alloy, $\alpha_1 = 0.9$–1.3; for materials containing precipitates and dispersoids, $\alpha_1 = 1.4$–1.8. In this study, we assume that the SiC reinforced aluminum alloy composites have a similar quenching strengthening mechanism as the materials with dispersoids. As the size of the SiC particles is large compared to the size of the dispersoids, we assume $\alpha_1 = 1.4$.

Recrystallization may occur by particle-stimulated nucleation during thermomechanical treatment for SiC reinforced aluminum alloy composites. Assuming that each SiC particle nucleates one grain, and then the grain size (D) and the increment of the yield stress (σ_{grs}) can be expressed as [8]

$$D = d\left[(1-f_p)/f_p\right]^{1/3} \quad (7)$$

$$\sigma_{grs} = K_y/D^{1/2}, \quad (8)$$

where $K_y = 0.1$ M N m$^{-3/2}$ is a constant [15].

Geometrically necessary dislocations are generated in the matrix during deformation. When SiC reinforced aluminum alloy composites are loaded, the particles deform less than the matrix. To avoid the initiation of the voids, dislocations are stored in the matrix to accommodate the deformed gradients and to allow compatible deformation of the particles and matrix. If the geometric-necessary dislocation array is a prismatic array, the increment of the yield stress can be expressed as [16]

$$\sigma_{gnds} = 2G(1-\upsilon)f_p\varepsilon/(1-2\upsilon), \quad (9)$$

where υ is Poisson's ratio of the matrix and ε is the tensile strain. In this study, ε is taken as the matrix yield strain, 0.002.

The modified shear lag model combining with the particle cracking and particle debonding

The modified shear lag model deals with an ideal condition, in which no particle cracking and particle debonding occur. In reality, both the particle cracking and particle debonding are generally observed in the SiC reinforced aluminum alloy composites during deformation [9–12, 17]. The particle cracking and particle debonding will inevitably decrease the yield stress of the composites since the

applied stress cannot be transferred from the matrix to the failed particles. Thus, the volume fraction of the SiC particles being used in the modified shear lag model is larger than the effective volume fraction of the SiC particles that can transfer the stress from the matrix to the hard reinforcements.

Particle debonding

Tohgo and Weng [18] showed that the probability of particle debonding in composites during deformation can be described by Weibull statistics, and that the debonding fraction (f_{de}) of the SiC reinforcements can be expressed as

$$f_{de} = 1 - \exp\left[-\left(\frac{\sigma_c}{P}\right)^m\right], \quad (10)$$

where σ_c is the stress on the reinforcements, P is the critical debonding normal stress function, and m is the Weibull constant with the value of 1–6. According to a previous study [19], the critical debonding stress function (P) can be expressed by the critical debonding stress (σ_d) and the critical debonding shear stress (τ_d) as follows:

$$P = 0.7\sigma_d \quad (11)$$

$$\sigma_d = 2\tau_d/n\coth(nA) \quad (12)$$

$$n = \left[\frac{E_m}{E_p(1+\upsilon)\ln(1/f_p)}\right]^{1/2}, \quad (13)$$

where A is the aspect ratio (defined as length/diameter), E_m and E_p are the matrix elastic modulus and reinforcement elastic modulus. Based on Nardin–Schultz model [20], the critical debonding shear stress can be expressed as

$$\tau_d = W_A(E_m/E_p)^{1/2}/\delta^{-1}, \quad (14)$$

Table 1 Summary of input data in the simulation

Parameters	Data	Comments
E_m (GPa)	67	Matrix elastic modulus
E_p (GPa)	460	SiC elastic modulus
G (GPa)	25.2	Matrix shear modulus
υ_m	0.33	Matrix Poisson's ratio
υ_p	0.17	SiC Poisson's ratio
V_0 (m^3)	1.78×10^{-14}	Reference volume of SiC particles
σ_0 (MPa)	1,550	Reference fracture strength of SiC particles
C_{Al} ($°C^{-1}$)	23.6×10^{-6}	Thermal expansion coefficient of Al
C_{SiC} ($°C^{-1}$)	4.3×10^{-6}	Thermal expansion coefficient of SiC
b (m)	2.86×10^{-10}	Magnitude of the Burgers vector
W_A (mJ m^{-2})	750	Interface bonding working

where δ^{-1}=0.5 nm is a constant and W_A is the work of adhesion, as shown in reference [20].

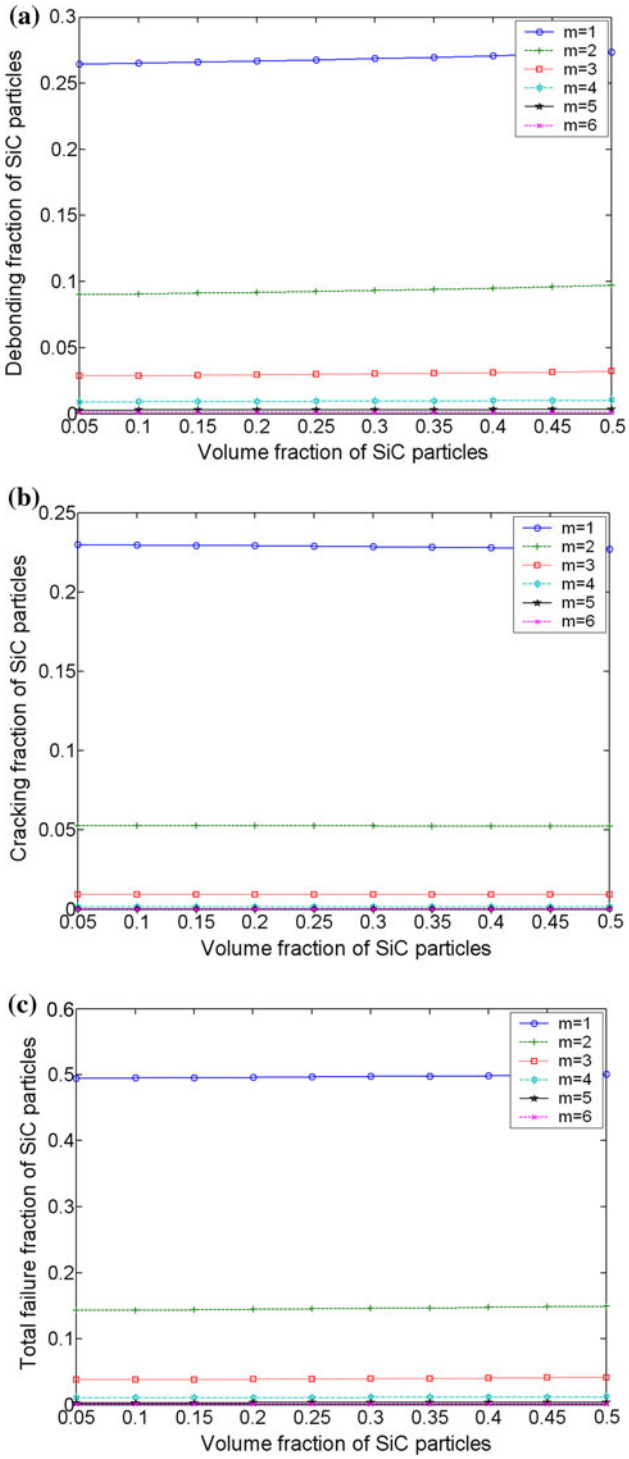

Fig. 1 Predicted **a** debonding, **b** cracking, and **c** total failure fractions of the SiC particles as a function of the volume fraction of SiC particles. All the calculated debonding fraction, cracking fraction, and total failure fraction of the SiC particles are at yield strain of 0.002. Note that m stands for the Weibull constant, and the size and the aspect ratio of the SiC particles are 20 μm and 1, respectively

Particle cracking

Lewis and Withers [10] indicated that the cracking fraction of the SiC particles in composites during deformation also follows the Weibull distribution and that the cracking fraction of the SiC particles can be expressed as

$$f_{cr} = 1 - \exp\left[-\frac{V_p}{V_0}\left(\frac{\sigma_c}{\sigma_0}\right)^m\right], \quad (15)$$

where σ_0 is the fracture strength of the SiC particles, V_p is the volume of the SiC particles, and V_0 is the volume of SiC particles for which the probability of survival is 37% at σ_0.

Determination of the internal stress on the SiC reinforcements

The determination of both particle cracking and particle debonding requires the internal stress on the SiC reinforcements be calculated. According to Withers et al. [13], the stress on the reinforcements, σ_c, can be calculated by externally applied stress through the Eshelby equivalent inclusion approach as follows:

$$\sigma_C = \sigma_I + \sigma_A + \sigma_{IM} = C_M\left(\varepsilon^c - \varepsilon^T\right) + C_M\varepsilon^A + C_M\varepsilon^M, \quad (16)$$

where σ_I is the stress due to the free shape change when the SiC particles are replaced by the matrix material, σ_A is the stress applied externally to the elastically homogeneous system, and σ_{IM} is the image stress in order to satisfy the boundary conditions at the external surfaces of a finite composite (for detailed descriptions of the above stresses readers are encouraged to refer to Withers et al. [13]), ε^A is the plastic strain of the matrix without reinforcements under a stress of σ_A; ε^c, ε^M, and ε^T are the constrained strain, the mean matrix strain and the equivalent homogeneous transformation strain, respectively, and C_M is the elastic constant (stiffness constant) of the matrix. For most materials the symmetry of the fourth rank stiffness tensor (elastic constant) enables its reduction to a 6 × 6 matrix (it is no longer strictly a tensor) and the stress and strain tensors to six element row or column vectors. According to Withers et al. [13], the constrained strain (ε^c), the mean matrix strain (ε^M), and the equivalent homogeneous transformation strain (ε^T) can be calculated as follows:

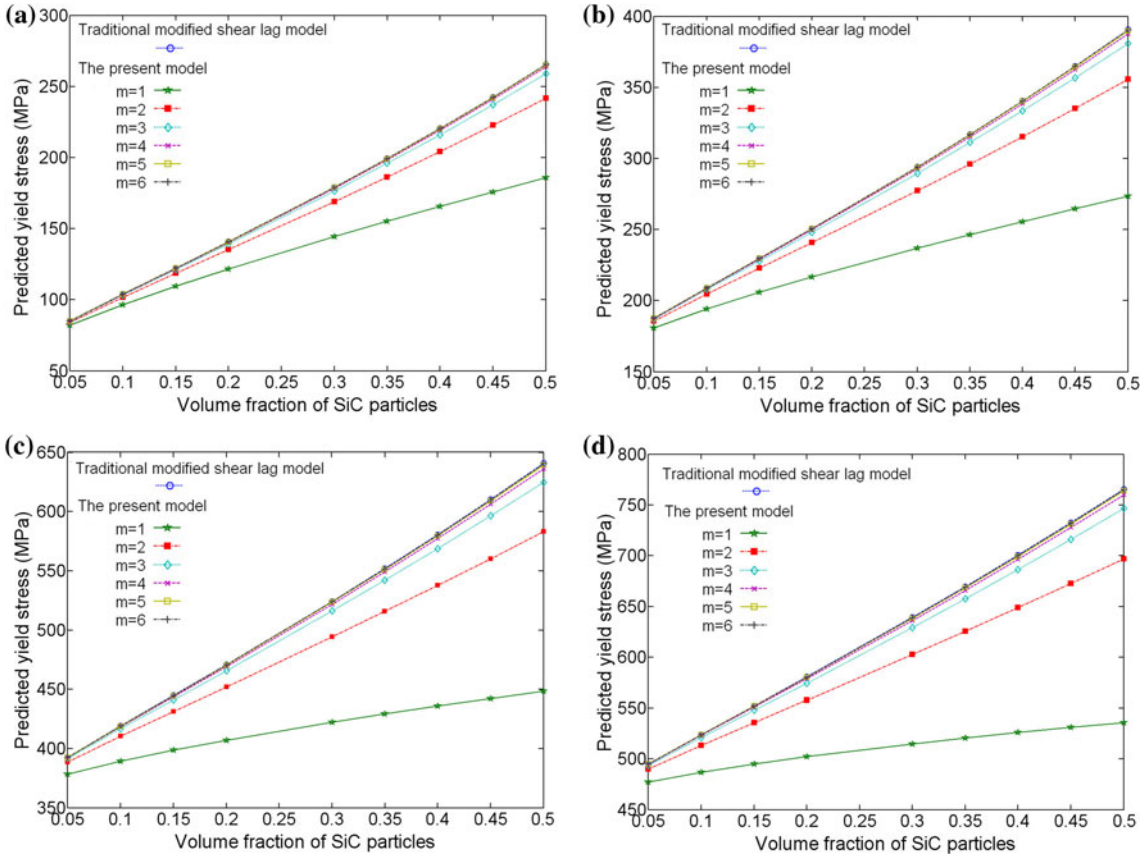

Fig. 2 Predicted yield stress as a function of the volume fraction of the SiC particles with the matrix intrinsic yield stresses of **a** 50, **b** 150, **c** 350, and **d** 450 MPa. Note that the size and the aspect ratio of the SiC particles are 20 μm and 1, respectively

$$\varepsilon^{T} = -[(C_M - C_P)[S - f_p(S - I)] - C_M]^{-1} \times [C_P\varepsilon^{T*} - (C_P - C_M)\sigma^{A}/C_M] \quad (17)$$

$$\varepsilon^{c} = S\varepsilon^{T} \quad (18)$$

$$\varepsilon^{M} = -f_p(S - I)\varepsilon^{T}, \quad (19)$$

where I is the identity tensor, S is the Eshelby tensor, and ε^{T*} is the free transformation strain of the inhomogeneous inclusion. It should be noted that the Eshelby tensor depends solely on the inclusion geometry and Poisson's ratio for the medium (for detailed information on the Eshelby tensor, readers are encouraged to refer to Brown and Clarke [21]). One should also note that for the loading of a previously unstressed composite $\varepsilon^{T*} = 0$, but $\varepsilon^{T} \neq 0$ in the above equations.

Modified shear lag model incorporating the particle cracking and particle debonding

As we discussed above, the applied stress cannot be transferred to the failed particles. Thus, the particle debonding and particle cracking will decrease the effective volume fraction of the SiC reinforcements. Then, the modified shear lag model incorporating the particle cracking and particle debonding can be expressed as

$$\sigma_{cy} = (\sigma_{in} + \sigma_{qs} + \sigma_{grs} + \sigma_{gnds})\{f_p[1 - f_{de} - (1 - f_{de})f_{cr}] \times (A + 2)/2 + f_m\} + \Delta\sigma_{or} \quad (20)$$

It should be noted that in Eq. 20, the contributing stress terms have different effects on the calculated yield stress of the composites. Orowan strengthening $\Delta\sigma_{or}$ can generally be ignored because SiC particles normally have relatively large size and Orowan strengthening can only have obvious effect when the particle size is in the range or less than a few microns. The other contributing terms, including the matrix intrinsic yield stress (σ_{in}), the quenching strengthening (σ_{qs}), the grain refinement strengthening (σ_{grs}), and the geometrically necessary dislocation strengthening (σ_{gnds}), have important effects on the calculated yield stress of the composites. However, it should be noted that the magnitudes of these effects depend on the volume fraction and granularity of SiC particles, as shown in a previous study [22].

Results

The model developed in the previous section was employed to carry out a parametrical study of the influence of the particle debonding and particle cracking on the yield stress of the composites. Both the aspect ratio, size and volume fraction of the SiC reinforcements have been considered in this work. The results from the traditional modified shear lag model, which does not consider the particle cracking and particle debonding, have also been

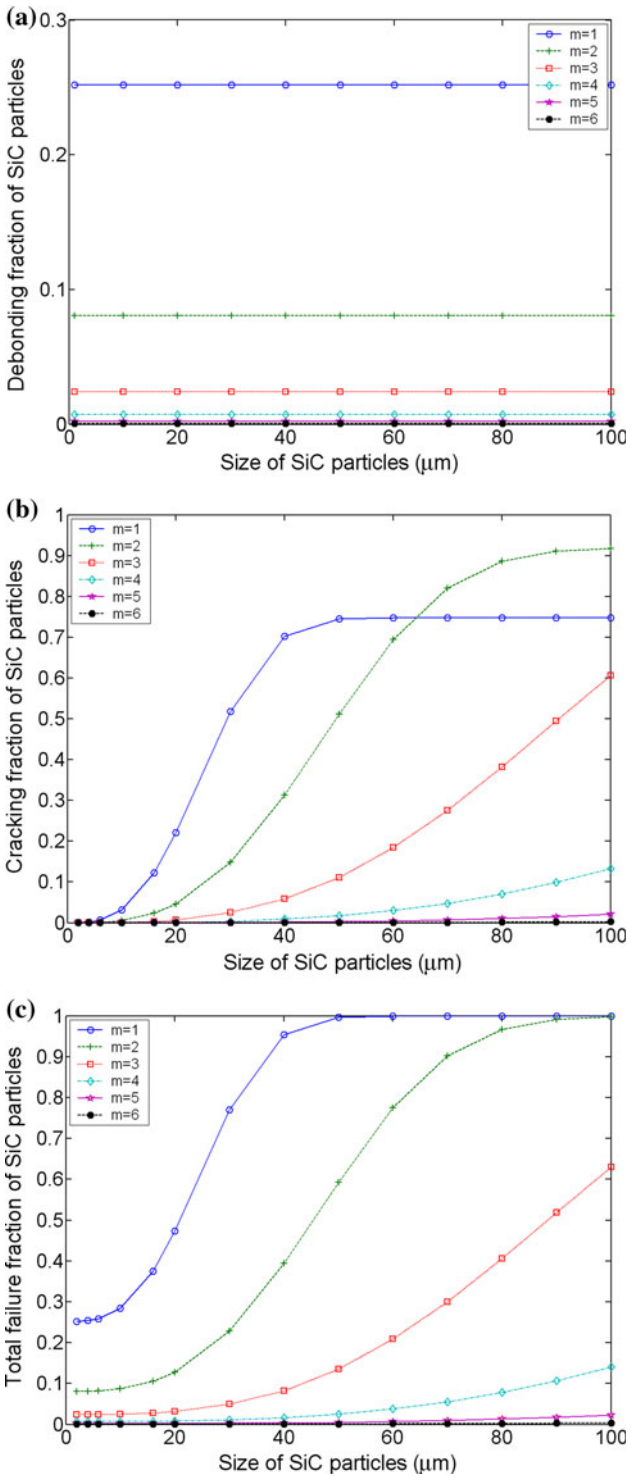

Fig. 3 Predicted **a** debonding, **b** cracking, and **c** total failure fractions of the SiC particles as a function of size of SiC particles. All the calculated debonding fraction, cracking fraction, and total failure fraction of the SiC particles are at yield strain of 0.002. Note that the volume fraction and aspect ratio of the SiC particles are 10% and 1, respectively

included to compare the present model. To calculate the yield stress of the SiC particle reinforced aluminum alloy composites, a series of the material parameters must be known, as shown in Table 1.

Influence of the volume fraction of SiC particles on the yield stress of the composites

Figure 1 shows the model predicted debonding fraction, cracking fraction, and total failure fraction of the SiC particles as a function of the volume fraction of the SiC particles. It should be noted that all the calculated debonding fraction, cracking fraction, and total failure fraction of the SiC particles are at the yield strain of 0.002. The SiC particles are assumed to be in round shape (aspect ratio of 1) and with the granularity of 20 μm. It can be seen from Fig. 1 that the debonding fraction and total failure fraction of the SiC particles increase slightly (almost constant) with the volume fraction of the SiC particles, while the cracking fraction of the SiC particles remains constant with the volume fraction of the SiC particles. It should be noted that the debonding fraction, cracking fraction, and total failure fraction of the SiC particles decrease as the Weibull constant (m) increases.

Figure 2 shows the model predicted yield stress of the composites with different matrix intrinsic yield stresses of 50, 150, 350, and 450 MPa as a function of the volume fraction of SiC particles. Here, the different matrix intrinsic yield stresses represent the typical values of pure aluminum, Al–Mg–Si, Al–Cu–Mg, and Al–Zn–Mg alloys. It can be seen from Fig. 2 that the yield stress of the composites increases with the volume fraction of the SiC particles, a phenomenon being generally observed for the SiC reinforced aluminum alloy composites [23]. In principle, the simulated yield stress of the composites by considering the particle debonding and particle cracking is lower than that of the composites without considering the particle debonding, no matter what value is the Weibull constant. This result is not surprising. As we discussed before, because the applied stress cannot be transferred to the failed SiC particles, there is a decrease in the effective volume fraction of the SiC particles and the yield stress of the composite. It should also be noted from Fig. 2 that the simulated yield stress of the composites decreases with the decrease in the

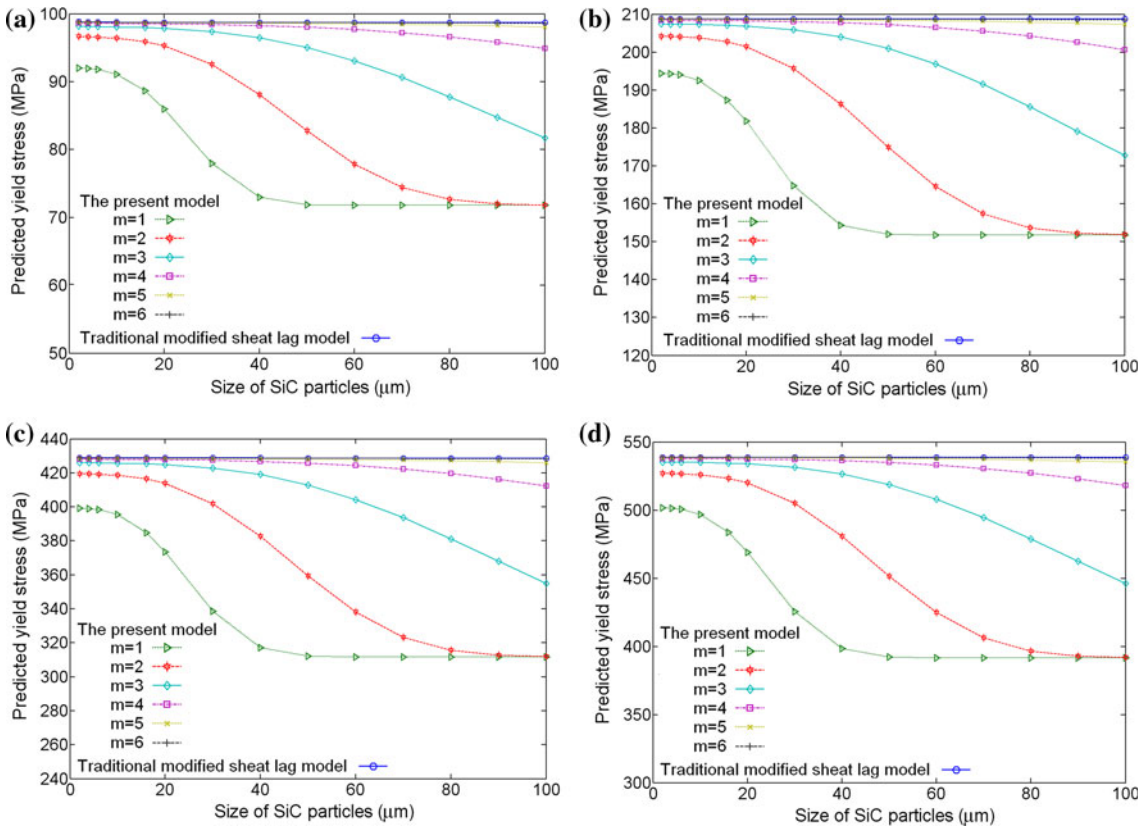

Fig. 4 Predicted yield stress as a function of size of the SiC particles with the matrix intrinsic yield stress of **a** 50, **b** 150, **c** 350, and **d** 450 MPa. Note that the volume fraction and aspect ratio of the SiC particles are 10% and 1, respectively

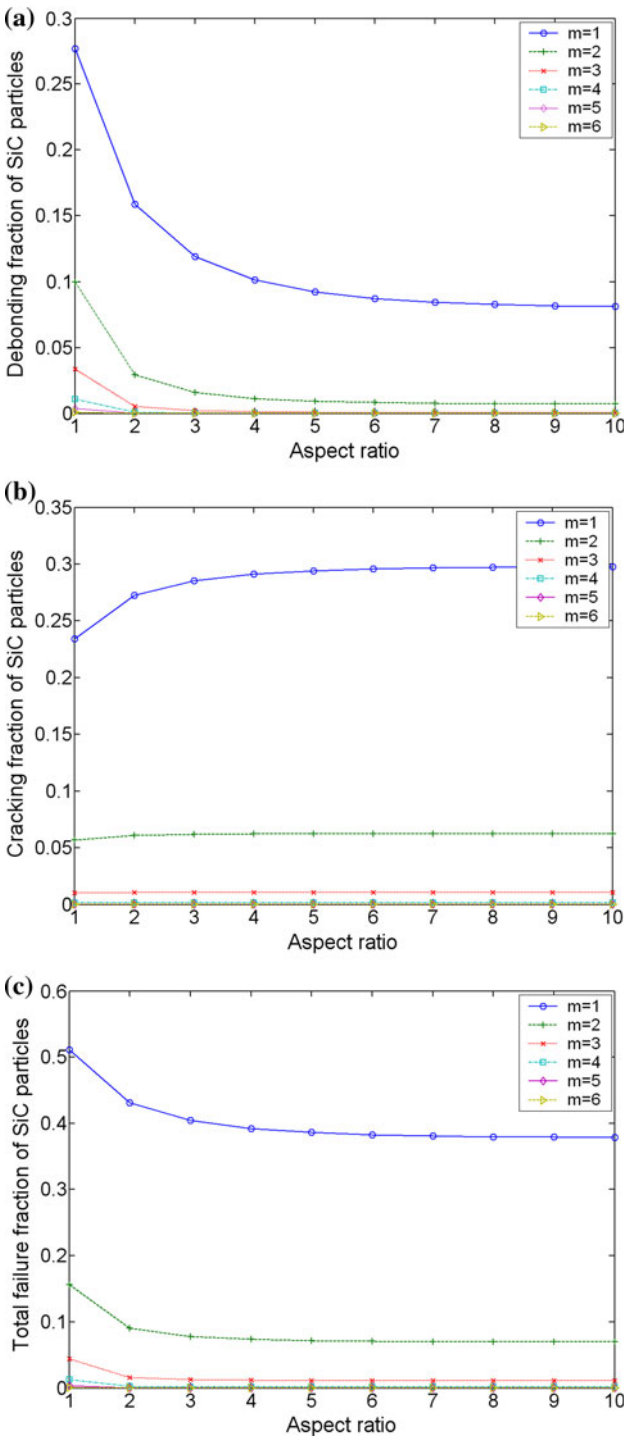

Fig. 5 Predicted **a** debonding, **b** cracking, and **c** total failure fractions of the SiC particles as a function of the aspect ratio of SiC particles. All the calculated debonding fraction, cracking fraction and total failure fraction of the SiC particles are at yield strain of 0.002. Note that the volume fraction and size of the SiC particles are 20% and 20 μm, respectively

Weibull constant value. According to Fig. 1, lower Weibull constant value results in a larger failure fraction of the SiC particles, thus a lower yield stress of the composites.

Influence of the size of the SiC particles on the yield stress of the composites

To study the effect of the particle size on the yield stress of the composites, we assume that the SiC particles are in round shape (aspect ratio of 1) and the volume fraction of the SiC particles is 10%. Figure 3 shows the model predicted debonding fraction, cracking fraction, and total failure fraction of the SiC particles as a function of the size of the SiC particles. All the calculated debonding fraction, cracking fraction, and total failure fraction of the SiC particles are at the yield strain of 0.002. It can be seen from Fig. 3 that the debonding fraction of the SiC particles remains constant with the size of the SiC particles, while the cracking fraction and total failure fraction of the SiC particles increase with the size of the SiC particles. This result indicates that the larger the size of the SiC particles, the higher the volume fraction of the failed SiC particles. In general, the particle debonding dominates the total failure fraction of the SiC particles when the particle size is small, while the particle cracking dominates the total failure fraction of the SiC particles when the particle size is large.

One should also note that the cracking fraction of the SiC particles with $m = 1$ is smaller than that of the SiC particles with $m = 2$ when the size of the particles is larger than about 60 μm. In general, interfacial debonding happens along weak interface at a relative low stress. Thus, the debonding fraction of the SiC particles are not included in the calculation of the cracking fraction of the SiC particles, resulting in the cracking fraction of the SiC particles when $m = 1$ being lower than that of the SiC particles when $m = 2$, on the condition that the particle size is larger than 60 μm. The larger debonding fraction of the SiC particles at $m = 1$, compared to $m = 2$, results in a lower unfailed volume fraction of the SiC particles before the particle cracking happens. However, no matter what is the particle size, the total failure fraction (sum of the debonding and cracking fractions) of the SiC particles increases as the Weibull constant value decreases.

Figure 4 shows the simulated yield stress of the composites with different matrix intrinsic yield stresses of 50, 150, 350, and 450 MPa as a function of the size of the SiC particles. It can be seen from Fig. 4 that the yield stress of the composites decreases as the size of SiC particles increases. In principle, the simulated yield stress of the composites by considering the particle debonding and particle cracking is lower than that of the composites without considering the particle debonding, no matter what is the Weibull constant value. As we discussed before, the applied stress cannot be transferred to the failed SiC particles, which results in a decrease in the effective volume fraction of the SiC particles and the yield stress of the composites. It should also be noted from Fig. 4 that the

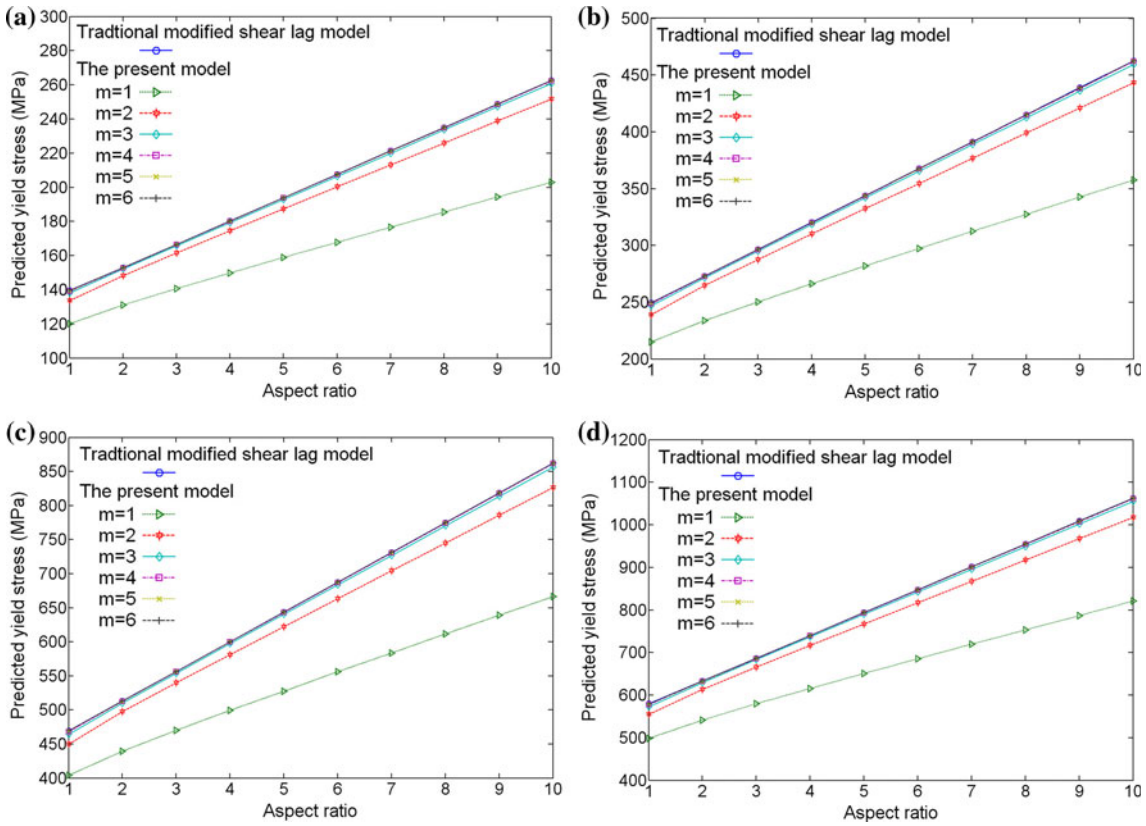

Fig. 6 Predicted yield stress as a function of the aspect ratio of the SiC particles with the matrix intrinsic yield stress of **a** 50, **b** 150, **c** 350, and **d** 450 MPa. Note that the volume fraction and size of the SiC particles are 20% and 20 μm, respectively

Table 2 Size and volume fraction of the SiC Particles used in the present study

Matrix types	Size of SiC (μm)	Volume fraction of SiC (%)
Pure aluminum	5, 10, 20, 30, 50	10, 15, 25, 35
Al–Mg–Si	5, 10, 20, 30, 45	7, 12, 20, 30, 45
Al–Cu–Mg	7, 15, 20, 30, 40	5, 15, 20, 35
Al–Zn–Mg	7, 15, 20, 30, 40	10, 15, 25, 35

simulated yield stress of the composites decreases with the decrease in the Weibull constant value. According to Fig. 3, lower Weibull constant value results in a larger total failure fraction of the SiC particles, thus also a lower yield stress of the composites.

Influence of the aspect ratio of the SiC particles on the yield stress of the composites

The effect of the aspect ratio of the SiC particle on the yield stress has also been calculated. In the simulation, the size and volume fraction of the SiC particles is assumed to be 20 μm and 20%, respectively. Figure 5 shows the debonding fraction, cracking fraction, and total failure fraction of the SiC particles as a function of the aspect ratio of the SiC particles. All the calculated debonding fraction, cracking fraction, and total failure fraction of the SiC particles are at the yield strain of 0.002. It should be noted that the SiC particles are assumed to be in round shape when the aspect ratio is 1, while they are assumed to be in cylindrical shape when the aspect ratio is larger than 1. The

Table 3 Parameters of the matrix alloys of the tested composites in the present work

Parameters	Elastic modulus (GPa)	Shear modulus (GPa)	Thermal expansion coefficient ($°C^{-1}$)	Poisson's ratio	Yield stress (MPa)
Pure aluminum	67	25.2	21.8×10^{-6}	0.33	53
Al–Mg–Si	69	25.6	22.5×10^{-6}	0.33	179
Al–Cu–Mg	70	25.9	22.1×10^{-6}	0.33	341
Al–Zn–Mg	72	26.7	23.5×10^{-6}	0.33	448

change of the aspect ratio from 1 to 10 results in a change in the Eshelby tensor, since the Eshelby tensor is different for spherical inclusions and cylindrical inclusions (the detailed value of the Eshelby tensor for spherical and cylindrical inclusions can be found from Brown and Clarke [21]). It can be seen from Fig. 5 that the debonding fraction of the SiC particles decreases with the aspect ratio of the SiC particles, while the cracking fraction of the SiC particles increases with the aspect ratio of the SiC particles. As a result of both particle debonding and particle cracking, the total failure fraction of the SiC particles decreases with the aspect ratio of the SiC particles, especially for the low value of the aspect ratio. This result indicates that the higher the aspect ratio of the SiC particles, the lower the volume fraction of the failure SiC particles. It should be noted that the debonding fraction, cracking fraction, and total failure fraction of the SiC particles decrease as the Weibull constant (m) increases, which indicated that smaller Weibull constant value results in a larger failure fraction of the SiC particles. Figure 6 shows the simulated yield stress of the composites with different matrix intrinsic yield stresses of 50, 150, 350, and 450 MPa as a function of the aspect ratio of the SiC particles. It can be seen from Fig. 6 that the yield stresses of the composites increase as the aspect ratio of SiC particles increases.

Experimental validation of the model

The accuracy of the model requires experimental validation. In the present work, four types of the typical aluminum alloy composites have been chosen to verify the model accuracy by varying the size and volume fraction of the SiC particles.

Experimental

Four types of the aluminum alloys, including 99.7% pure aluminum, Al–4.7%Mg–0.3%Si, Al–4.5%Cu–0.6%Mg, and Al–6.4%Zn–2.3%Mg (weight percentage) alloys, were selected as the matrix materials to study the yield stress of the SiC reinforced aluminum alloy composites and to verify the model accuracy. The matrix composite billets reinforced with various sized and volume fractioned SiC particles were produced by the powder metallurgy (P/M) process. The sizes and volume fractions of the SiC particles used in the present study are shown in Table 2. The P/M billets were converted into rods by hot extrusion with an extrusion ratio of 9:1. The extruded rods of the composites were solution heat treated for 10 h at 420 °C in a salt bath furnace followed by cold water quenching to the room temperature. No aging treatment has been applied to the composites to avoid the effect of the precipitates on the yield stress of the composites. The yield stresses of the composites were measured by tensile testing, which was performed on all solution treated samples. At room

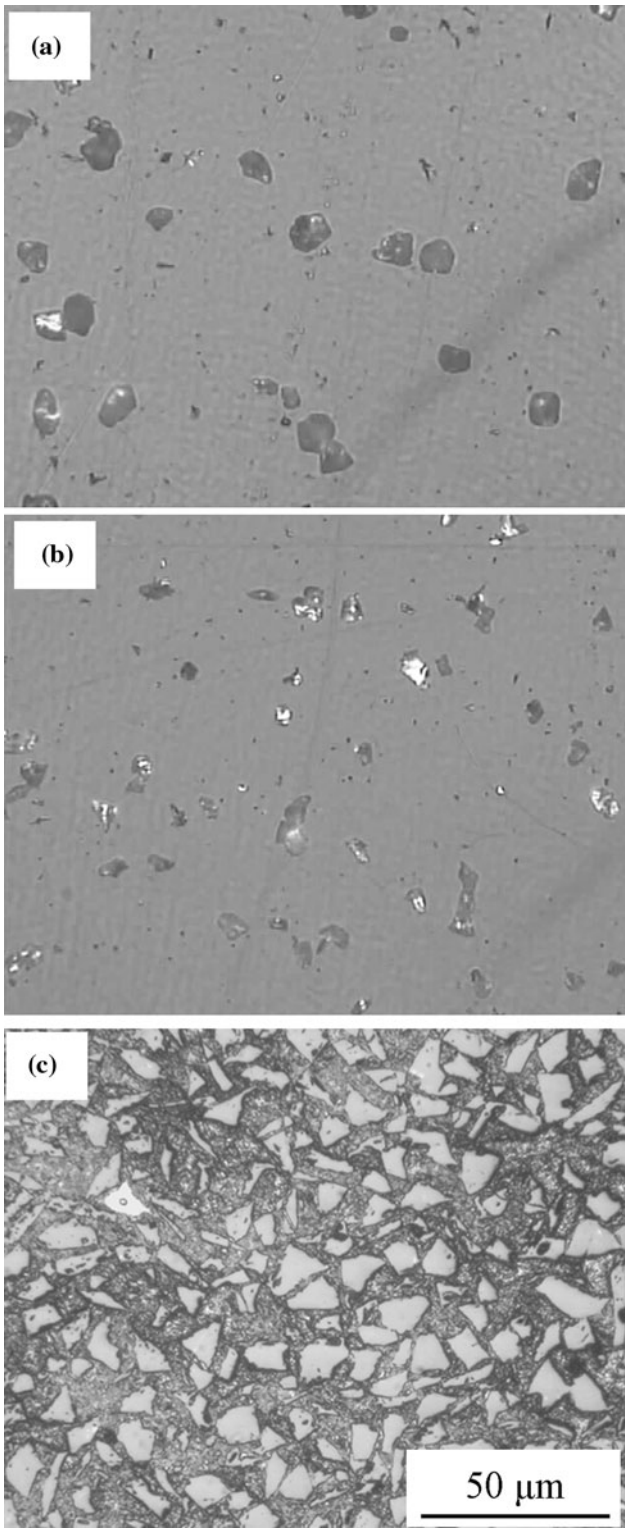

Fig. 7 Distribution of SiC particles in Al–Mg–Si alloy matrix, **a** 10 μm in size and 7% in volume fraction, **b** 5 μm in size and 7% in volume fraction, and **c** 10 μm in size and 45% in volume fraction

temperature, dog-bone-shaped tensile specimens from all solution treated alloys, having a gage size of 6 mm in diameter and 40 mm in length, were served in the tensile test at a constant strain rate of 5×10^{-4} s^{-1} on an Instron 8802 testing machine. The yield stress was determined as the 0.2 pct offset. All the yield stresses of the specimens are the average value of three to five testing results. For the model simulations, we used the parameters shown in Table 3. The SiC particles used in the present work have the same parameters as shown in Table 1.

The microstructures of the composites have been investigated using optical microscopy. Figure 7 shows a typical distribution of different volume fractioned and sized SiC particles (aspect ratio of 1) in the Al–Mg–Si alloy. It can be seen that the SiC particles are uniformly distributed in the matrix without particle aggregation. In reality, the distributions of SiC particles in all four types of the matrix alloys are nearly uniform, without much aggregation.

Comparison of the experimental data with the model predictions

It should be noted that the values of the parameter m used in the calculation of the yield stress of different matrix composites are based on the results of the microstructural observations, as shown in Figs. 8 and 9. It can be seen from Figs. 8 and 9 that the model predicted fractions of the particle debonding and cracking agree well with the experimental counterparts if the proper m values are chosen. Figures 10 and 11 show the model predicted yield stresses of the composites and the experimental counterparts as a function of the volume fraction and size of the SiC particles, respectively. The yield stresses predicted by the traditional modified shear lag model have also been included for comparison. Figures 10 and 11 show that the present model predicted yield stresses agree well with the experimental counterparts, while the traditional modified shear lag model predicted yield stresses are obviously higher than the experimental counterparts, especially when the volume fraction and size of the SiC particles are large. This result indicates that the present model fits the experiments better than the traditional modified shear lag model. Figure 10 shows that the yield stress of the SiC reinforced aluminum alloy composites increases as the volume fraction of the SiC particles increases, no matter what is the matrix material. Figure 11 shows that the yield stress of the SiC reinforced aluminum alloy composites decreases as the size of the SiC particles increases. For the traditional

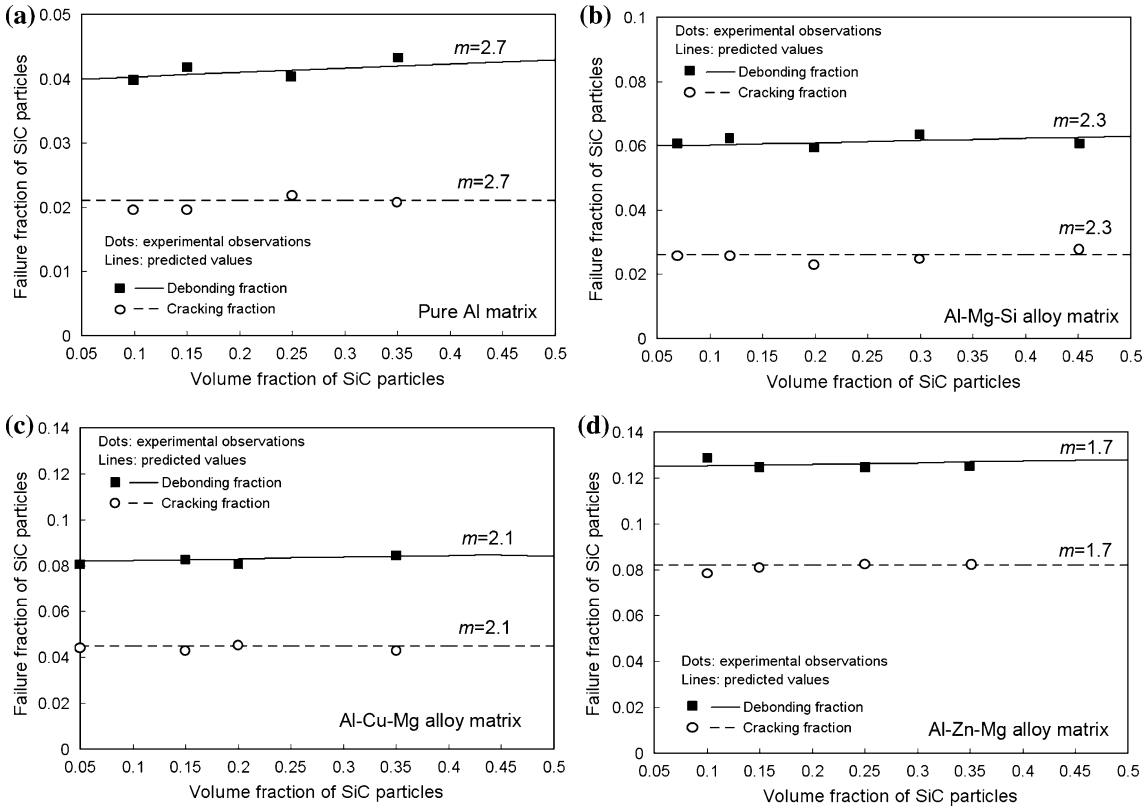

Fig. 8 Simulated and experimental determined failure fractions of the SiC particles as a function of the volume fraction of SiC particles, with the matrix of **a** pure aluminum, **b** Al–Mg–Si, **c** Al–Cu–Mg, and **d** Al–Zn–Mg alloys. All the calculated debonding fraction and cracking fraction of the SiC particles are at yield strain of 0.002. Note that the size and the aspect ratio of the SiC particles are 20 μm and 1, respectively (*lines*: predicted values, *dots*: experimental data)

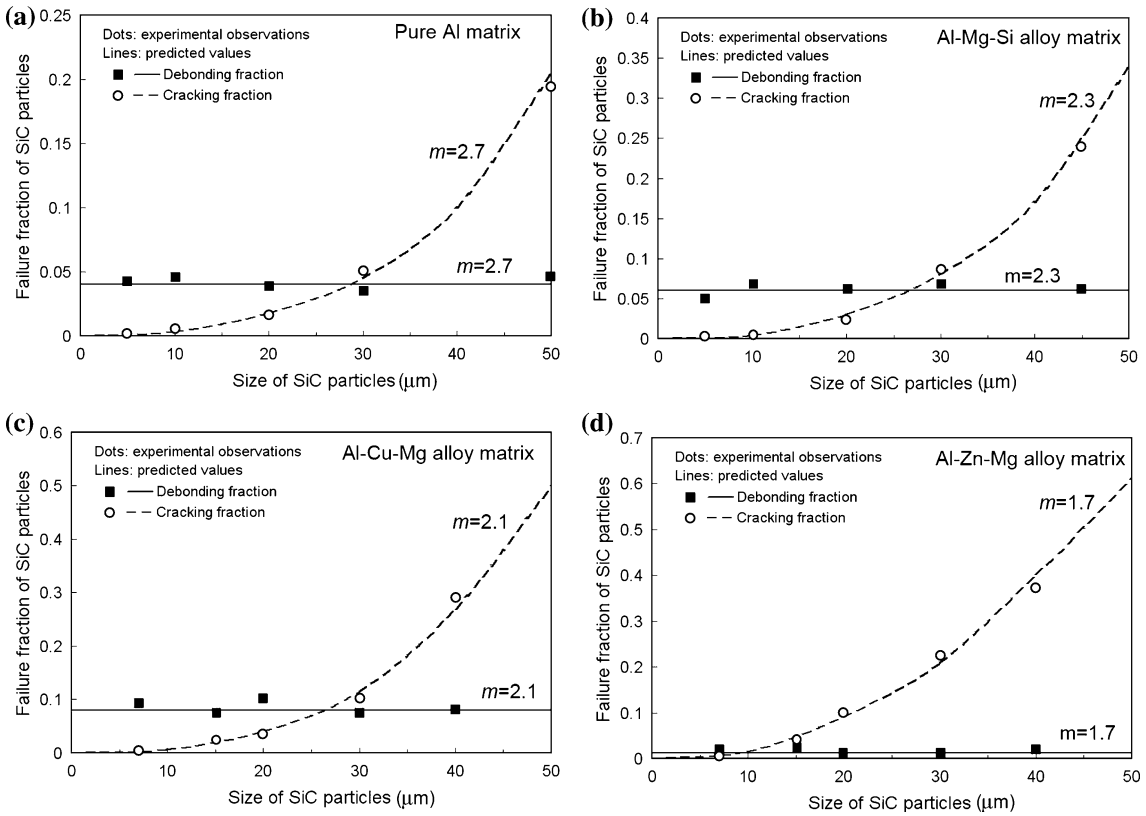

Fig. 9 Simulated and experimental determined failure fractions of the SiC particles as a function of the size of SiC particles, with the matrix of **a** pure aluminum, **b** Al–Mg–Si, **c** Al–Cu–Mg, and **d** Al–Zn–Mg alloys. All the calculated debonding fraction and cracking fraction of the SiC particles are at yield strain of 0.002. Note that the volume fraction and the aspect ratio of the SiC particles are 10% and 1, respectively (*lines*: predicted values, *dots*: experimental data)

modified shear lag model, the predicted yield stress is independent of the SiC particle size, while for the present model, the predicted yield stress of the composites decreases as the size of the SiC particles increases, which agrees well with the experiments.

Discussion

In general, the yield stress of the composites increases as the volume fraction and aspect ratio of the SiC particles increase, but it decreases as the size of the SiC particles increases. The increase of the yield stress of the composites with the aspect ratio has been verified by the previous studies, in which the SiC whisker reinforced aluminum alloy composites show a higher yield stress, compared to the SiC platelet reinforced aluminum alloy composites under the same other conditions (same volume fraction, hot working, and heat treatment procedure). It should be noted that the yield stress of the SiC whisker reinforced composites is anisotropic (under the condition that the SiC whiskers are oriented preferentially), while the yield stress of the SiC platelet reinforced composites is isotropic. For equivalent SiC volume fraction, the yield stress of the SiC whisker reinforced composites in the longitudinal direction is greater than that of the SiC platelet reinforced composites [3]. Previous studies [11, 12, 24] also indicated that the yield stress of the composites increases as the size of the SiC particles decreases. For a given volume fraction of the SiC particles, smaller particles result in a larger interfacial surface between the matrix and the particles, and thus increase the load being transferred to the SiC particles and also fewer SiC particles fracture, which inevitably increases the yield stress of the composites. The traditional modified shear lag model predictions show a similar trend of the relationship between yield stress with the size, volume fraction, and aspect ratio of the SiC particles, as the present model predictions, but always with higher values, especially for the composites with larger volume fraction, size, and aspect ratio. The main difference between the traditional modified shear lag model and the present model is that the present model incorporates the particle debonding and particle cracking in the simulation, and thus results in a lower effective volume fraction of the SiC particles and the simulated yield stress. As the size and volume fraction of the SiC particles increase, the volume

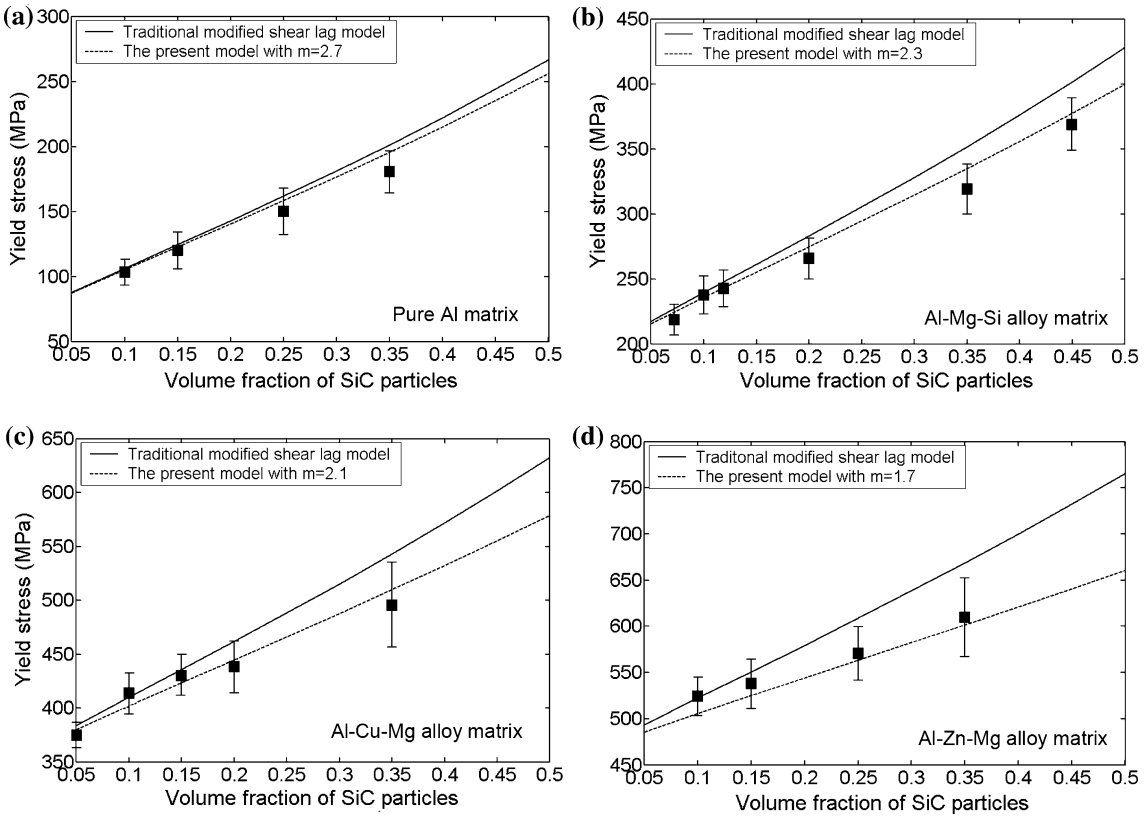

Fig. 10 Simulated and experimental determined yield stresses as a function of the volume fraction of the SiC particles, with the matrix of **a** pure aluminum, **b** Al–Mg–Si, **c** Al–Cu–Mg, and **d** Al–Zn–Mg alloys. Note that the size and aspect ratio of the SiC particles are 20 μm and 1, respectively (*lines*: predicted values, *dots*: experimental data)

fraction of the failed SiC particles increases, and thus the difference between the traditional modified shear lag model and the present model simulated yield stresses increases. Since the particle failure is an intrinsic phenomenon in the composites during deformation, the present model simulations agree much better with the experimental counterparts than the traditional modified shear lag model simulations.

The effects of the matrix materials on the yield stress of the composites depend not only on the intrinsic yield stress, but also on the Weibull constant. Figures 10 and 11 show that as the intrinsic yield stress of the matrix alloy increases, the Weibull constant used in the model simulation decreases, which indicated that higher matrix intrinsic yield stress results in a larger failure fraction of the SiC particles during deformation. In reality, lower Weibull constant means higher failure fraction of the SiC particles. According to the shear lag theory, the load is transferred from the matrix to the hard SiC particles during deformation. Higher matrix intrinsic yield stress results in a larger load being transferred to the SiC particles, thus, a higher volume fractioned debonding and cracking fraction of the SiC particles.

It should be noted that the experiments in the present work did not apply aging treatment on the composites after solution and quenching treatments. In most aluminum alloy composites, yield stress will change during aging because of the second phase precipitates nucleation and growth. Compared to the aluminum alloys, the SiC reinforced aluminum alloy composites exhibit aging acceleration phenomenon [25–28]. The aging acceleration behavior of the composites is caused by the heterogeneous nucleation and growth of the precipitates along the dislocations, which are generated during solution and quenching treatments because of the large difference in thermal expansion between the aluminum alloy matrix and the SiC reinforcements. In the present model, for simplicity, we did not consider aging hardening behavior of the composites during annealing. However, aging hardening behavior and aging acceleration phenomenon have been quantified in a previous study [22].

It should be noted that during the calculation of the grain refinement strengthening (σ_{grs}) the assumption of one SiC particle nucleating one grain is very simple. The recrystallization and grain size changing by the addition of the SiC particles are very complicated topics, which are beyond the

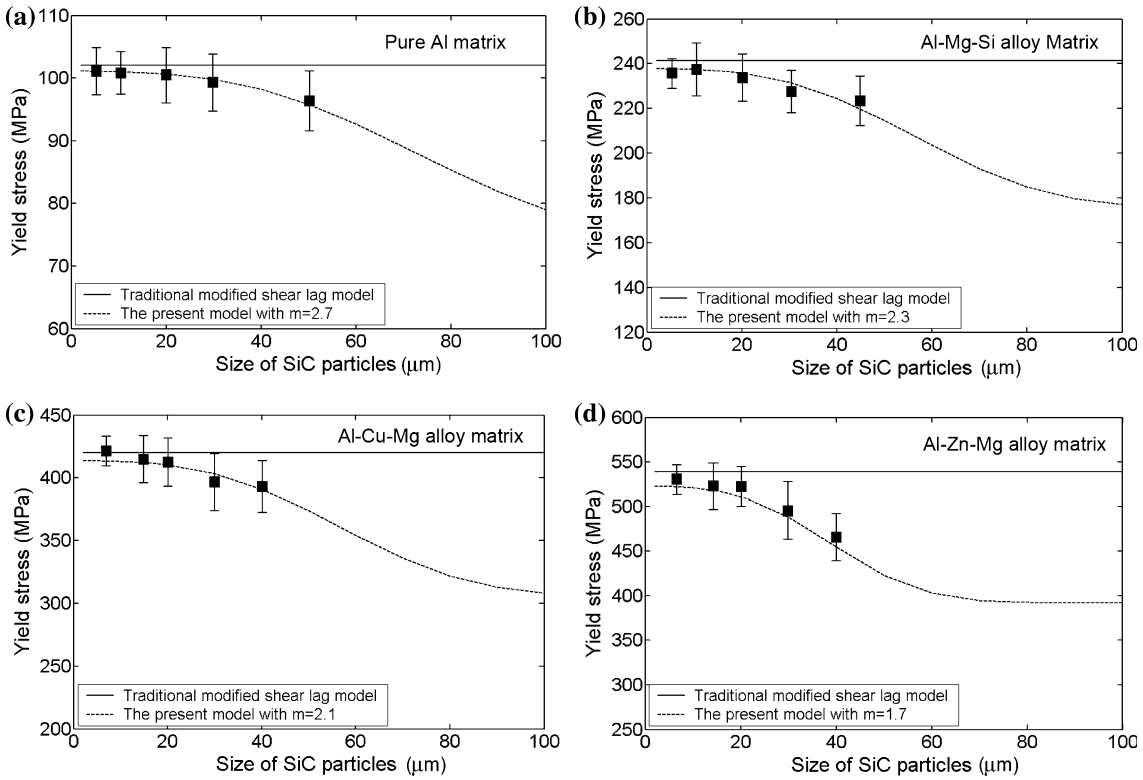

Fig. 11 Simulated and experimental determined yield stresses as a function of the size of the SiC particles, with the matrix of **a** pure aluminum, **b** Al–Mg–Si, **c** Al–Cu–Mg, and **d** Al–Zn–Mg alloys. Note that the volume fraction and aspect ratio of the SiC particles are 10% and 1, respectively (*lines*: predicted values, *dots*: experimental data)

topic of this article. Here, we used this previously published assumption [8] to calculate the grain size in this work for simplicity, as shown in Eqs. 7 and 8. It should also be noted that the incremental contributions to yield stress of the composites are assumed to be additive in this work, as described in Eq. 4. However, this is a simple assumption and it is not so clear whether the incremental contributions to yield stress should be additive or not at this stage. Here, we assumed that they should be additive for simplicity. One more thing should be noted is that the Weibull constants in Eqs. 10 and 15 do not required to be the same, but only depend on the experimental observations. In this study, we found that two constant are similar based on the microstructural observations, as shown in Figs. 8 and 9.

Conclusion

In this article, a constitutive model including the particle debonding and cracking for the yield stress of the SiC reinforced aluminum alloy composites has been developed based on the modified shear lag model, the Eshelby's equivalent inclusion approach and the Weibull statistics. The model simulation indicates that the yield stress of the composites increases with the volume fraction and aspect ratio of the SiC particles increase, but it decreases as the size of the SiC particles increases. Four types of the aluminum alloy, including pure aluminum, Al–Mg–Si alloy, Al–Cu–Mg alloy, and Al–Zn–Mg alloy, have been chosen as the matrix materials to verify the model accuracy. It has been shown that the model predictions agree well with the experimental counterparts, which indicates that the model can be used to predict the yield stress of the composites. The model, which considers the particle debonding and particle cracking during deformation, fits the experimental data much better than the traditional modified shear lag model.

Acknowledgements This work was supported by National Natural Science Foundation of China (50801068), PhD Programs Foundation of Ministry of Education of China (200805331044), and Hunan Postdoctoral Scientific Program (2008RS4020). One of the authors would also like to thank the support from Chinese Postdoctoral Science Foundation (200801345, 20070410303).

References

1. Cox HL (1952) Br J Appl Phys 3:72
2. Kelly A (1973) Strong solids. Clarendon Press, Oxford, p 147
3. Nardone VC (1987) Scr Metall 21:1313
4. Nardone VC, Prewo KM (1986) Scr Metall 20:43

5. Taya M, Arsenault RJ (1987) Scr Metall 21:349
6. Arsenault RJ, Fisher RM (1983) Scr Metall 17:67
7. Arsenault RJ, Shi N (1986) Mater Sci Eng 81:175
8. Miller WS, Humphreys FJ (1991) Scr Metall Mater 25:33
9. González C, Llora J (1996) Scr Mater 35:91
10. Lewis CA, Withers PJ (1995) Acta Metall Mater 43:3685
11. Llorca J (1995) Acta Metall Mater 43:181
12. Maire E, Wilkinson DS, Embury JD, Fougeres R (1997) Acta Mater 45:5261
13. Withers PJ, Stobbs WM, Pedersen OB (1989) Acta Metall 37:3061
14. McElro TJ, Szkopiak ZC (1972) Inter Metall Rev 17:175
15. Sekine H, Chen R (1995) Composites 26:183
16. Ashby MF (1970) Philos Mag 21:399
17. Liews CA, Stobbs WM, Withers PJ (1993) Mater Sci Eng A 171:1
18. Tohgo K, Weng GJ (1994) Trans ASME J Eng Mater Technol 116:414
19. Lee HK (2001) Comp Mech 27:504
20. Shimbo M, Naka M, Okamoto I (1989) J Mater Sci Lett 8:663
21. Brown LM, Clarke DR (1975) Acta Metall 23:821
22. Song M, Li X, Chen KH (2007) Metall Mater Trans A 38:638
23. Hong S, Kim H, Huh D, Suryanarayana C, Chun BS (2003) Mater Sci Eng A 347:198
24. Arsenault RJ, Wang L, Feng CR (1991) Acta Metall Mater 39:47
25. Dutta I, Bourell DL (1989) Mater Sci Eng A 112:67
26. Nieh TG, Karlak RF (1984) Scr Metall 18:25
27. Papazian JM (1988) Metall Trans A 19:2945
28. Varma VK, Mahajan YR, Kutumnarao VV (1997) Scr Mater 37:485